Modeling of combined effects of divertor closure and advanced magnetic configuration on detachment in DIII-D by SOLPS

H. Si[1], H. Y. Guo[2], B. Covele[2], A.W. Leonard[2], J.G. Watkins[3], and D. Thomas[2]
[1] Institute of Plasma Physics Chinese Academy of Sciences, Hefei, Anhui, China
[2] General Atomics, San Diego, California, USA
[3] Sandia National Laboratories, Albuquerque, NM, USA

E-mail: hsi@ipp.cas.cn (H. Si) and guohy@fusion.gat.com (H. Y. Guo)

Abstract
One of the major challenges facing the design and operation of next-step high-power steady-state fusion devices is to develop a divertor solution for handling power exhaust, while ensuring acceptable divertor target plate erosion, which necessitates access to divertor detachment at relative low main plasma densities compatible with current drive and high plasma confinement. Detailed modeling with SOLPS is carried out to examine the effect of divertor closure on detachment with the normal single null divertor (SD) configuration, as well as one of the advanced divertor configurations, such as X-divertor (XD) respectively. The SOLPS modeling for a high confinement plasma in DIII-D finds that increasing divertor closure with SD reduces the upstream separatrix density at the onset of detachment from $1.18\times10^{19}\,m^{-3}$ to $0.88\times10^{19}\,m^{-3}$. Moreover, coupling the divertor closure with XD further promotes the onset of divertor detachment at a still lower upstream separatrix density, down to the value of $0.67\times10^{19}\,m^{-3}$, thus, showing that divertor closure and advanced magnetic configuration can work synergistically to facilitate divertor detachment.

Keywords : divertor, detachment, modeling, DIII-D

1. Introduction

It is one of the grand challenges to control the heat flux and erosion at the divertor target plates for high performance, steady-state plasma operation. In general, developing an advanced divertor configuration requires: 1) increasing divertor closure by divertor baffling to improve divertor screening for recycling neutrals and impurities, hence increasing divertor neutral pressure, thus enhancing divertor particle and power exhaust; 2) optimizing magnetic configuration to extend the plasma-wetted area through flux expansion, and increase the divertor volume by increasing the field-line length [1-9].

DIII-D features a comprehensive diagnostic set, flexible divertor geometry and wide range of boundary plasma parameter space [10], thus providing a capable platform for developing and validating advanced divertor solutions. Promising progress has been made on DIII-D in exploring impacts of divertor closure and advanced magnetic configurations, such as X-Divertor (XD) and snowflake divertor (SFD), on divertor

detachment, leveraging DIII-D's flexible poloidal field coils and robust control system, to provide insight and guidance for the development of a fully optimized divertor concept in DIII-D [7, 11]. Previous XD experiments in DIII-D found considerable benefits over Standard Divertor (SD) geometries, both for divertor target heat flux density reduction and detachment facilitation [12]. This paper reports on the combined effects of divertor closure and advanced magnetic configuration on divertor detachment and energy dissipation in DIII-D by detailed modeling using the SOLPS code for both SD and XD magnetic configurations with different divertor closure in a typical H-mode plasma condition. The rest of the paper is organized as follows. Section 2 describes the key input parameters used in SOLPS modeling. In section 3 comparisons by SOLPS modeling are made in detail between SD and XD with different divertor closure on divertor plasma detachment onset and heat flux density on the divertor target. Section 4 contains the summary and conclusion.

2. SOLPS model

DIII-D can vary the divertor closure of the lower divertor by placing the outer striking point (OSP) on the shelf as an open divertor, and on the floor as a relatively more closed divertor to improve neutral trapping and impurity screening in the divertor. Figure 1 shows four different divertor geometries with SD and XD magnetic configurations, respectively: SD-shelf (a) and XD-shelf (c) are the SD and XD magnetic configurations with the OSP on the shelf of the lower divertor of DIII-D, while SD-floor (b) and XD-floor (d) refer to the SD and XD with the OSP on the floor.

SOLPS modeling was carried out for the different diverter configurations in DIII-D, as shown in Fig. 1. The SOLPS code package consists of a multi-fluid plasma code B2/B2.5 for ions and electrons at each ionization state and a kinetic Monte-Carlo code Eirene for neutral solver for the plasma edge of tokamaks including the outer core edge, scrape-off layer (SOL), and divertor regions, taking into account detailed atomic processes, such as collision, ionization, and recombination [13-28]. All of the calculations presented in this paper are carried out by SOLPS5.1 [29]. In contrast to SOLPS5.0, SOLPS5.1 includes n-n collisions, which requires triangular mesh between the plasma region and the wall. In the modeling, the radial-poloidal plasma distributions on a representative poloidal cross-section of DIII-D are sampled by the computational mesh including plasma grid (blue) and triangular grid (green), as shown in figure 1.

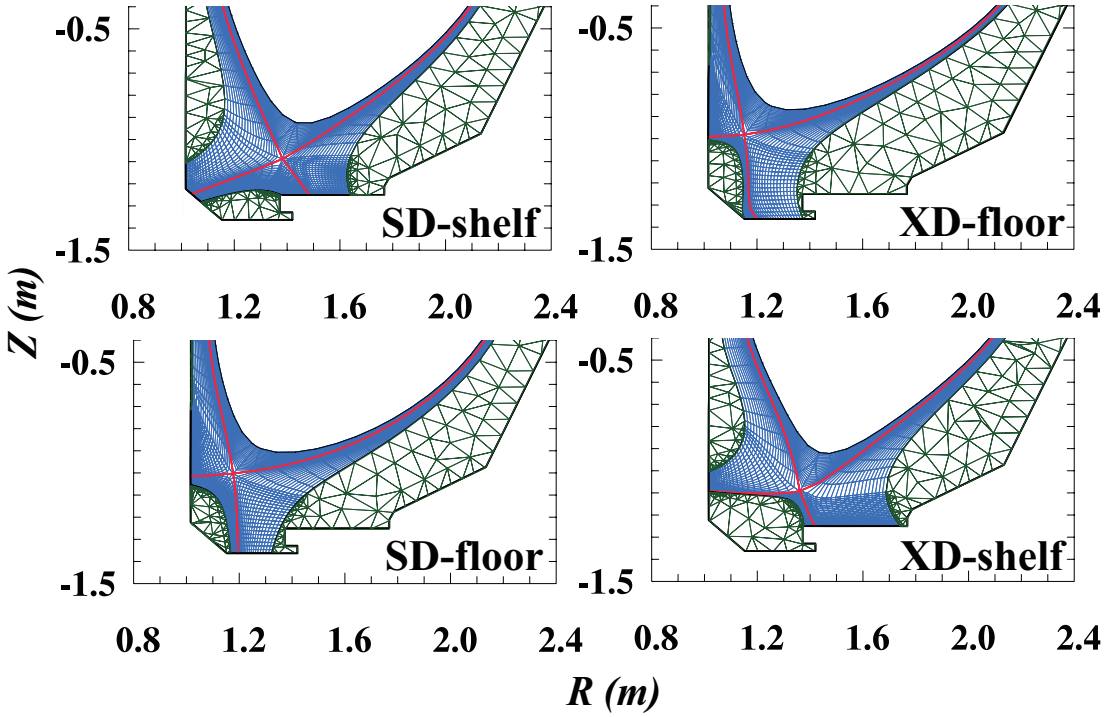

Figure 1. The physical meshes of SOLPS5.1 including triangular mesh for four different DIII-D divertor configurations: (a)SD-shelf, (b)SD-floor, (c)XD-shelf and (d) XD-floor.

At the innermost boundary, at $r - r_{sep} = -1.0cm$ of OMP, the density, $n_{D^+,core}$, is fixed at various values. Both deuterium plasma species (D^0, D_2^0, D^+, D_2^+) and carbon impurities (C^0, C^+, C^{2+}, C^{3+}, C^{4+}, C^{5+}, C^{6+}) are considered in the simulations. Physical sputtering yield is based on the modified Roth-Bohdansky formula [30, 31] and chemical sputtering yield is set to be constant as 0.02 on the carbon surface. The cross-field transport coefficients for anomalous ion and electron thermal conduction, $\chi_{\perp i,e}$, and anomalous particle density diffusivity, $D_\perp$, are provided to SOLPS as input parameters, which can be radially adjusted to fit experimental profiles. Drifts are not considered in this work.

3. Results and discussions

3.1. SOLPS cross-field transport coefficients

In order to identify appropriate cross-field transport coefficients for SOLPS modeling, we first modeled an H-mode discharge (#160563) in DIII-D as the reference condition. The radial profiles of $D_\perp$ and $\chi_{\perp i,e}$ used in the SOLPS code, as shown in figure. 2, are determined by systematically matching the upstream profiles of electron density n_e, electron temperature T_e measured by Edge Thomson Scattering (ETS) at the outer midplane (OMP), as well as the outer target profiles of n_e, T_e, parallel particle flux density $\Gamma_{||}$ and parallel heat flux density $q_{||}$ measured by Langmuir probes at the divertor targets, as shown in figure 3. These transport coefficients are used as common input parameters for all the SOLPS simulations to compare the four different kinds of

divertor configurations, i.e., (a)SD-shelf, (b)SD-floor, (c)XD-shelf and (d)XD-floor respectively.

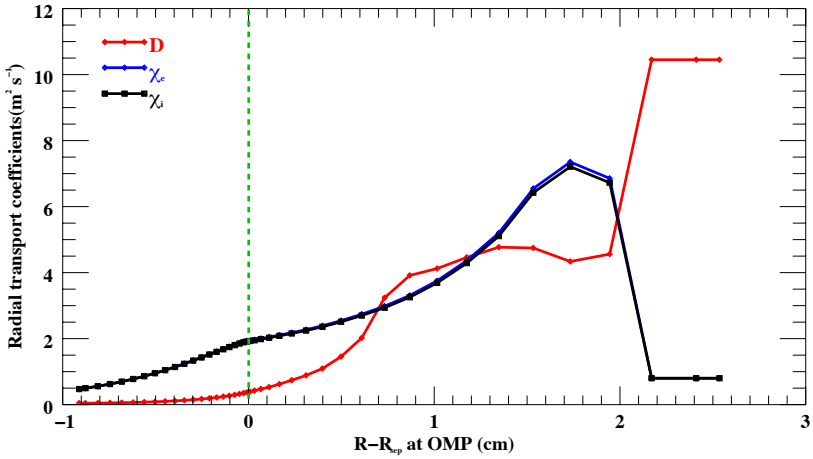

Figure 2. Cross-field transport coefficients ($D_\perp$, $\chi_{\perp e}$, $\chi_{\perp i,}$) used in SOLPS5.1

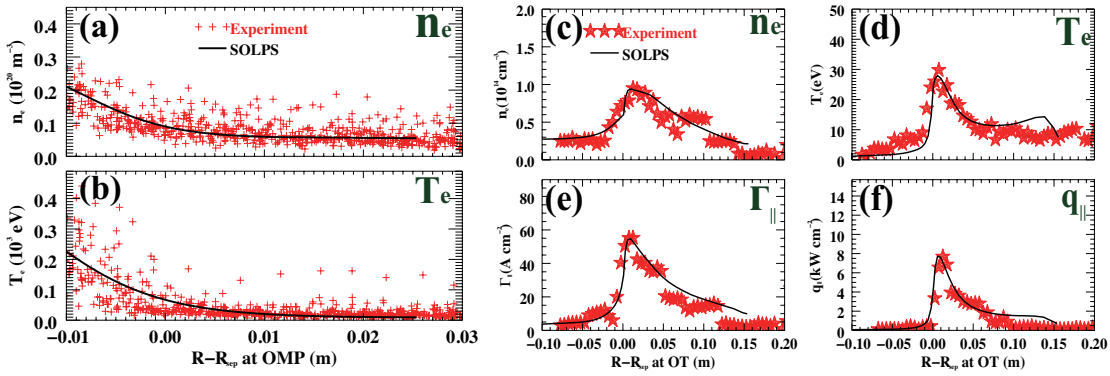

Figure 3. The experimental (#160563) and SOLPS5.1 calculated upstream profiles of (a)n_e, (b)T_e at OMP and outer target profiles of (c) n_e, (d) T_e, (e) $\Gamma_{||}$ and (f) $q_{||}$.

3.2. Effect of divertor closure with SD on plasma detachment

For the SD-shelf configuration, the OSP is on the shelf without any divertor baffling, so that the lower outer divertor can be treated as a fully open divertor. In contrast, the SD-floor configuration features a more closed divertor structure with the OSP on the floor near the baffle. With the common transport coefficients shown in figure 2, the direct comparisons between SD-shelf and SD-floor are made to assess the influence of the different divertor closure with SD on plasma detachment in DIII-D. Figure 4 shows the radial profiles of n_e and T_e at the OMP, and parallel heat flux density at the divertor entrance (at the X-point) $q_{||}^{divent}$, calculated by SOLPS5.1, for a specific

upstream density, $n_{e,sep}^{OMP} = 1.02\times10^{19}\ m^{-3}$, and input power, $P_{i,\ sep} = P_{e,\ sep} = 1.725$ MW at the separatrix of OMP.

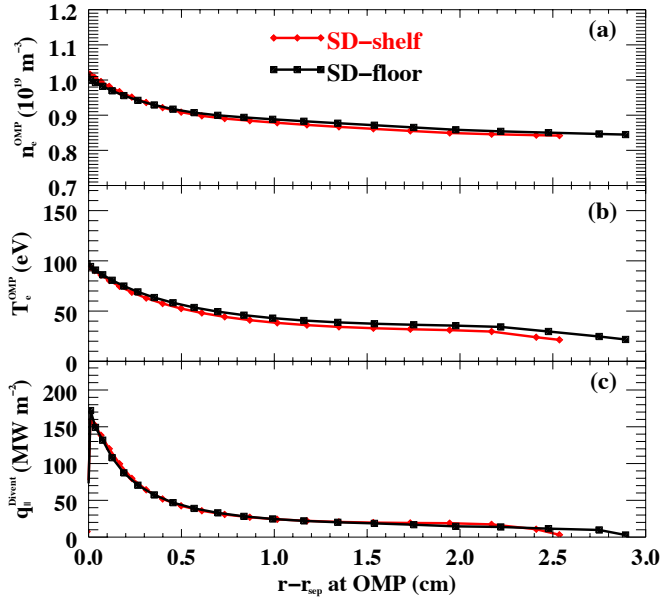

Figure 4. Radial profiles of (a) n_e and (b) T_e at the OMP, (c) $q_{||}^{divent}$ for SD-shelf and SD-floor configurations with the upstream density $n_{e,sep}^{OMP} = 1.02\times10^{19}\ m^{-3}$.

As can be seen, the upstream profiles of n_e and T_e, as well as the $q_{||}$, are similar for both divertor configurations. Figure 5 compares the corresponding divertor target profiles along the lower outer divertor between SD-shelf and SD-floor: (a) n_{et}, (b) atoms (deuterium and carbon) density $n_{(D+C)t}$, (c) T_{et}, (d) deuterium molecule density n_{D2t}, (e) perpendicular heat flux density q, (f) parallel heat flux density $q_{||}$. It is clear that in figure 5 (c) the peak value of T_{et} for SD-shelf, 28 eV, is much higher than that for SD-floor, 2eV. Moreover, the peak value of q in figure 5 (e) is reduced from 2.1 MW/m^2 for SD-shelf to 0.6 MW/m^2 for SD-floor. The peak value of n_{et} in figure 5 (a) for SD-shelf is about $0.9\times10^{20}\ m^{-3}$, much lower than that for SD-floor, $3.7\times10^{20}\ m^{-3}$. It appears that the more closed SD-floor configuration can more effectively trap neutrals with significantly higher $n_{(D+C)t}$ and n_{D2t}. The peak value of $n_{(D+C)t}$ increases from $0.2\times10^{19}\ m^{-3}$ for SD-shelf to $3.9\times10^{19}\ m^{-3}$ for SD-floor, as shown figure 5 (b), while n_{D2t} increases from $0.3\times10^{19}\ m^{-3}$ for SD-shelf to $1.8\times10^{19}\ m^{-3}$ for SD-floor, as shown in figure 5 (d). Figure 6 shows the 2D distributions of n_{D2} and T_e for both SD-shelf and SD-floor with the same specific upstream density, $n_{e,sep}^{OMP} = 1.02\times10^{19}\ m^{-3}$, as aforementioned. It appears that the

neutrals are preferentially trapped at the bottom of the lower outer target by the baffle for SD-floor, thus promoting divertor power dissipation with the T_{et} near the lower outer target being much lower than that for SD-shelf.

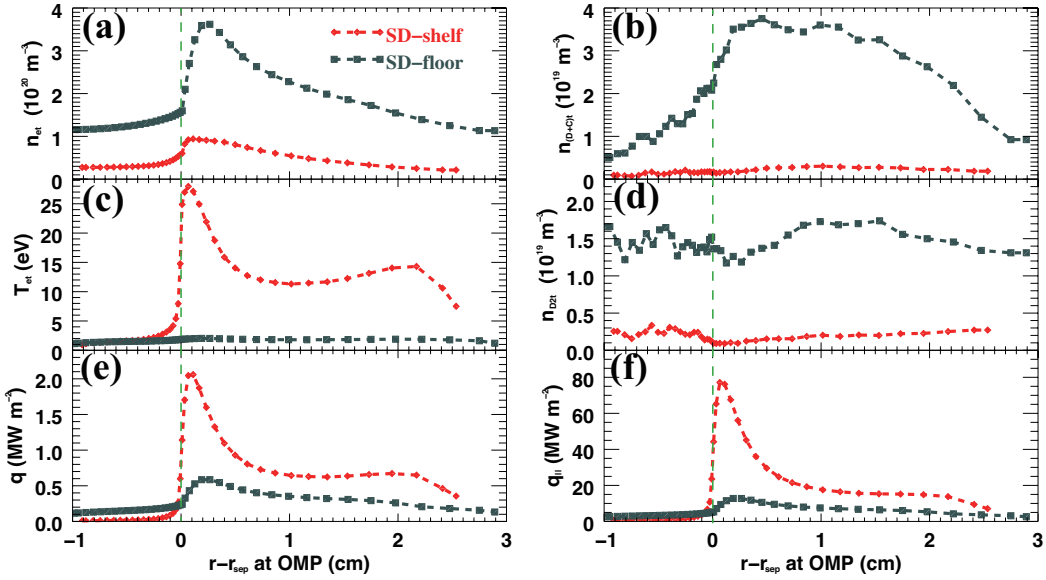

Figure 5. Radial profiles of (a) n_{et}, (b)$n_{(D+C)t}$, (c) T_{et}, (d) n_{D2t}, (e) q and (f) $q_{||}$ along the lower outer divertor target for both SD-shelf and SD-floor configurations, $n_{e,sep}^{OMP} = 1.02\times10^{19}\ m^{-3}$.

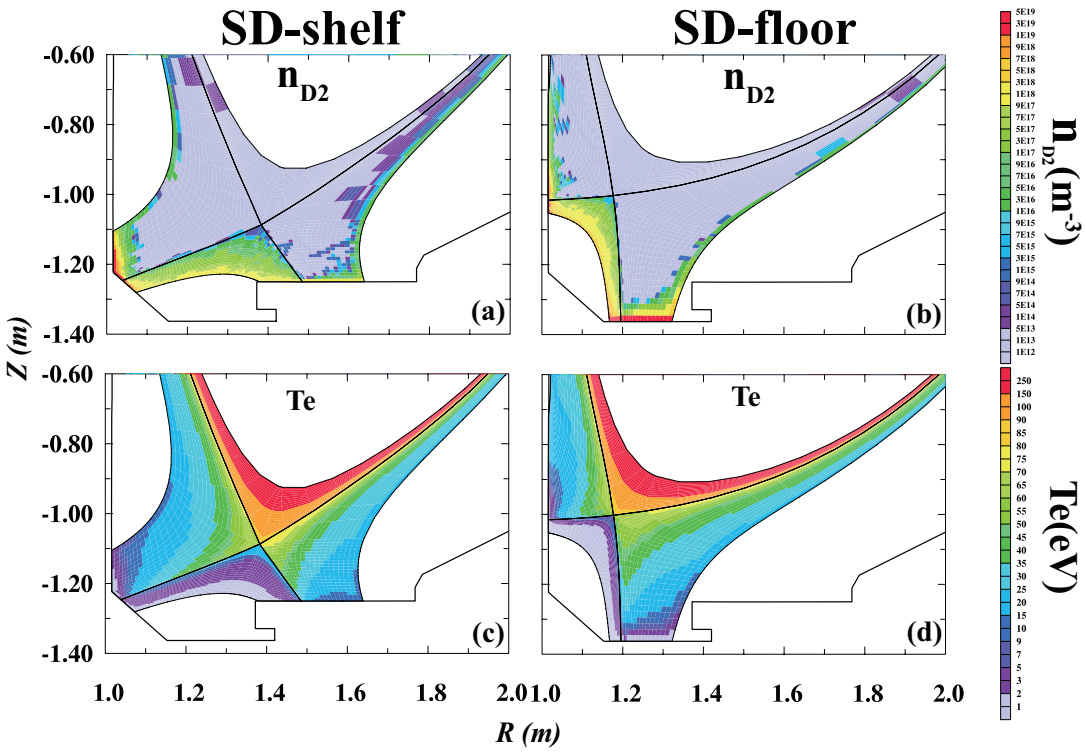

Figure 6. 2D distributions of n_{D2} and T_e for both SD-shelf and SD-floor with upstream density $n_{e,sep}^{OMP} = 1.02\times10^{19}\ m^{-3}$

To determine the onset of detachment, a systematic scan of the separatrix density at OMP, $n_{e,sep}^{OMP}$, was carried out for both SD-floor and SD-shelf. In figure 7 the electron temperature (T_e^{OSP}), parallel particle flux density ($\Gamma_{||}^{OSP}$), heat flux density (q^{OSP}) at OSP are plotted as a function of $n_{e,sep}^{OMP}$. As can be seen, as $n_{e,sep}^{OMP}$ increases, T_e^{OSP} for both SD-shelf and SD-floor decreases. In contrast to the SD-shelf configuration, T_e^{OSP} for the SD-floor configuration exhibits a more pronounced decrease, down to ~ 1 eV at a lower upstream separatrix density, which indicates that the more closed SD-floor configuration facilitates divertor plasma detachment, presumably due to more effective neutral trapping (figure 6). The rollover of parallel particle flux density is usually used as an indicator for the onset of detachment. Figure 7 (b) shows that the parallel particle flux density rollover starts at $0.88\times10^{19}\ m^{-3}$ for SD-floor and $1.18\times10^{19}\ m^{-3}$ for SD-shelf respectively. It is interesting to note that, because the plasma-wetted area of the lower outer target for the open SD-shelf configuration without any baffling is larger than that for the more closed SD-floor configuration (by ~84%), the energy flux density q^{OSP} for SD-shelf is smaller than that for SD-floor at lower upstream separatrix density. However, as the upstream density, $n_{e,sep}^{OMP}$ increases sufficiently, owing to the stronger energy dissipation by neutrals, SD-floor quickly enters detachment, with the corresponding q^{OSP} rapidly decreasing, down to the level below the SD-shelf case, in spite of smaller flux expansion, as mentioned above.

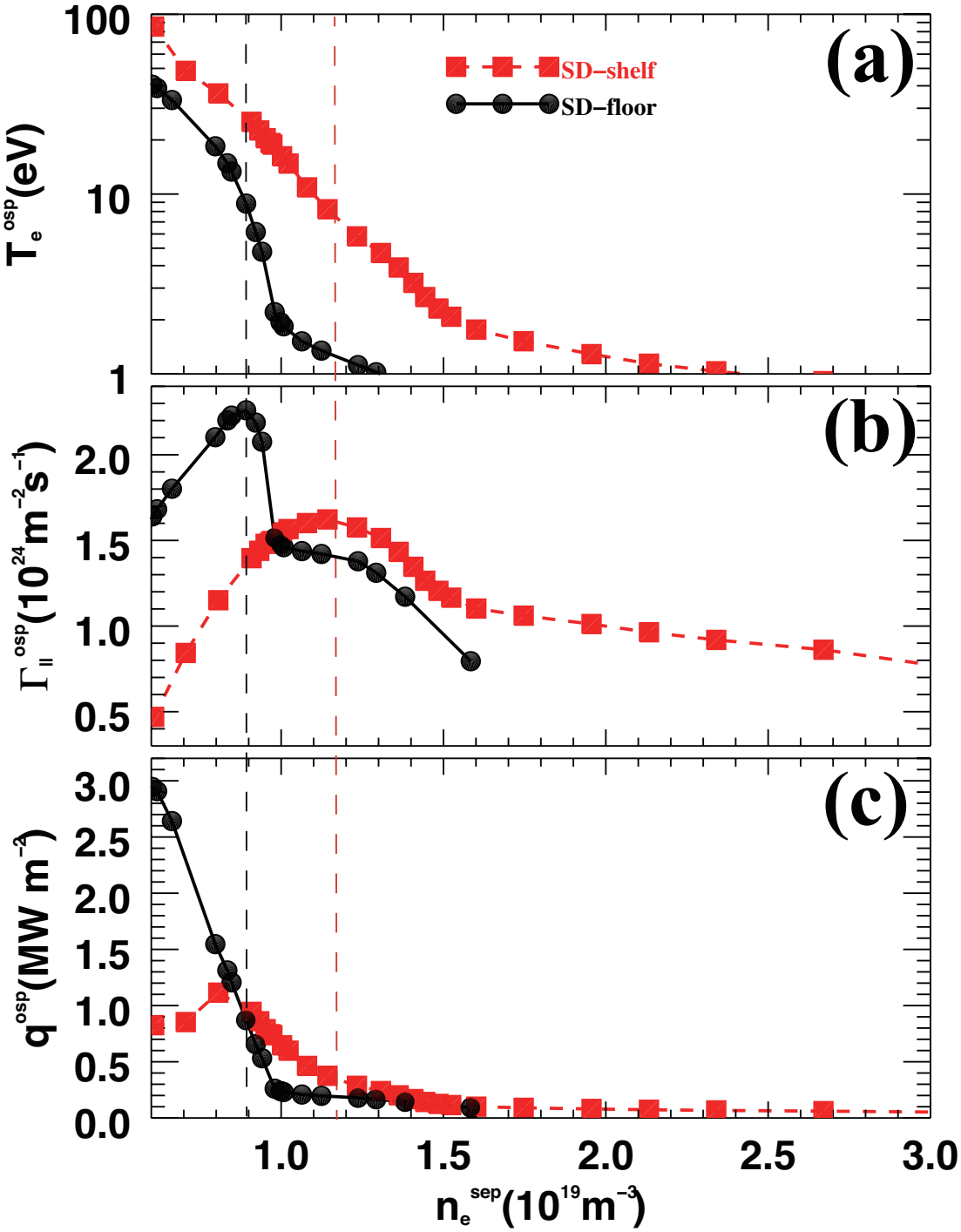

Figure 7. (a)T^{osp}, (b)$\Gamma_{||}^{OSP}$, (c) q^{OSP} at the OSP as a function of the upstream density $n_{e,sep}^{OMP}$ for both SD-shelf and SD-floor, as predicted by SOLPS.

3.3. Coupling of divertor closure with XD on plasma detachment

SOLPS modeling has also been made to access synergistic effects of divertor closure and advanced magnetic configuration, i.e., XD. Figure 8 shows the radial profiles of n_e and T_e at the OMP, and $q_{||}^{divent}$ for a specific upstream density at OMP, $n_{e,sep}^{OMP} = 1.05\times10^{19}$ m^{-3}, for both XD-shelf and XD-floor configurations.

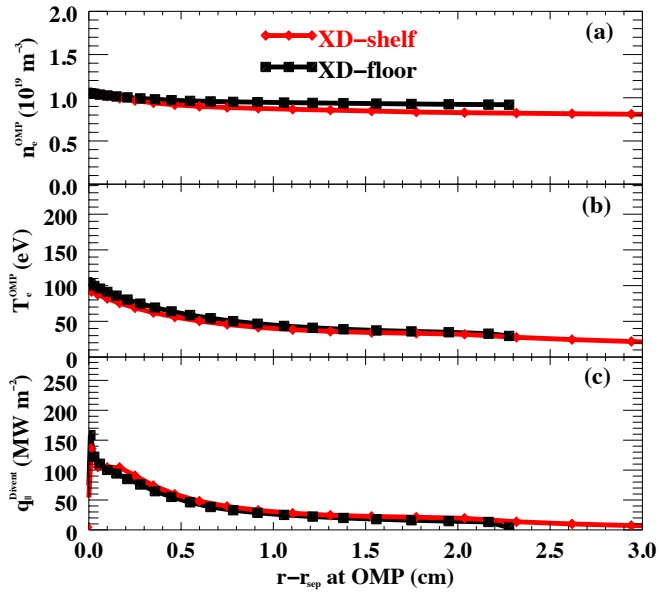

Figure 8. Radial profiles of (a) n_e and (b) T_e at the OMP, (c) $q_{||}^{divent}$ for XD-shelf and XD-floor with the upstream density $n_{e,sep}^{OMP} = 1.05\times10^{19}$ m^{-3}.

Figure 9 shows the profiles of (a) n_{et}, (b) $n_{(D+C)t}$, (c) T_{et}, (d)n_{D2t}, (e) q and (f) $q_{||}$ along the lower outer divertor target for XD-shelf and XD-floor at the specific upstream density, $n_{e,sep}^{OMP} = 1.05\times10^{19}$ m^{-3}. As shown in figure 9 (c) that the peak value of T_{et} for XD-shelf, 38.6 eV, is much higher than that for XD-floor, 2.3 eV. Moreover, the peak value of q in figure 9 (e) is reduced from 0.95 MW/m^2 for XD-shelf to 0.2 MW/m^2 for XD-floor. The peak value of n_{et} in figure 9 (a) for XD-shelf is about 1.55×10^{20} m^{-3}, which is much lower than that for XD-floor, 3.35×10^{20} m^{-3}.

Similar to the SD configuration, the more closed XD-floor configuration can trap neutrals more effectively than the XD-shelf configuration, as clearly shown in the figures 9 (b) and (d). The peak value of $n_{(D+C)t}$ increases from 0.4×10^{19} m^{-3} for XD-shelf to 3.2×10^{19} m^{-3} for XD-floor and n_{D2t} increases from 0.57×10^{19} m^{-3} for XD-shelf to 5.14×10^{19} m^{-3} for XD-floor. Figure 10 shows the 2D distributions of n_{D2} and T_e for both XD-shelf and XD-floor at the same upstream density $n_{e,sep}^{OMP} = 1.05\times10^{19}$ m^{-3}, which clearly shows that the neutral density is enhanced by the baffle in XD-floor, compared to XD-shelf. Note, however, that due to larger flux expansion in XD, the XD configurations are less effective at trapping neutrals than SD configurations, especially near the separatrix and in the private flux region, as shown in Figures 6 and 10.

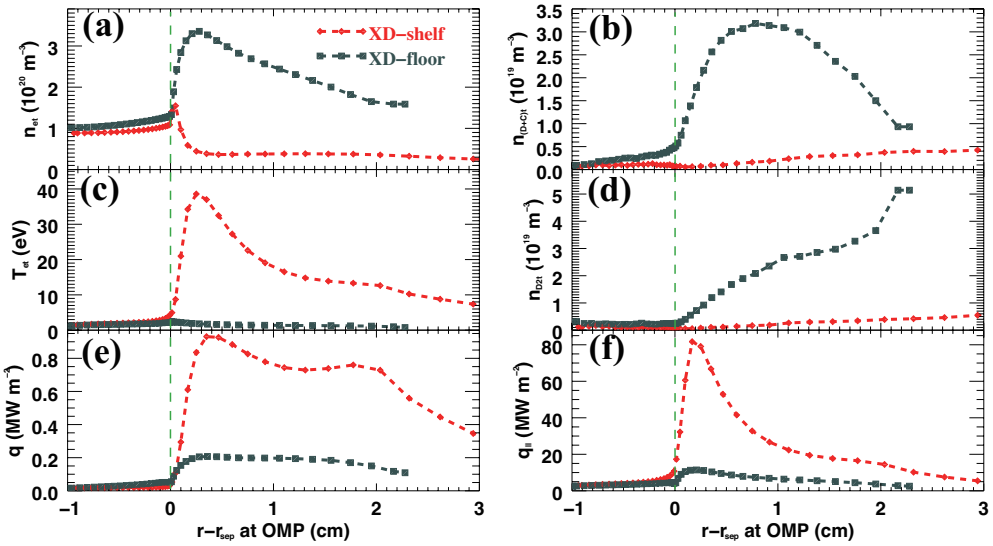

Figure 9. Profiles of (a) n_{et}, (b)$n_{(D+C)t}$, (c) T_{et}, (d) n_{D2t}, (e) q and (f) $q_{||}$ along the lower outer divertor target for both XD-shelf and XD-floor

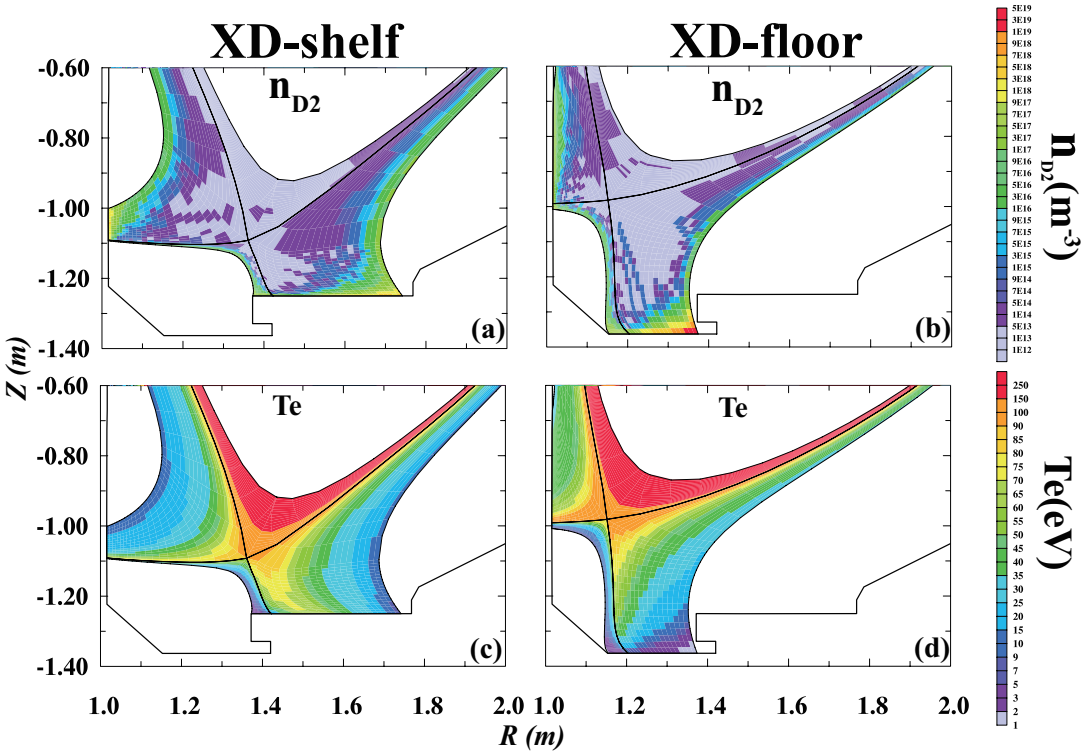

Figure 10. 2D distributions of n_{D2} and T_e for both XD-shelf and XD-floor with upstream density $n_{e,sep}^{OMP} = 1.05\times10^{19}\ m^{-3}$

Figure 11 shows T_e^{OSP}, $\Gamma_{||}^{OSP}$ and q^{OSP} at OSP as a function of $n_{e,sep}^{OMP}$. As $n_{e,sep}^{OMP}$ increases, T_e^{OSP} for both XD-shelf and XD-floor configurations decreases. Similar to the SD configurations, T_e^{OSP} for XD-floor also shows a faster decrease, due to increased divertor closure, figure 11(a), compared with XD-shelf. However, the difference is less pronounced than that for SD cases, resulting from relatively lower neutral trapping efficiency. Similar to the SD cases, because the plasma-wetted area of the lower outer target for XD-shelf without any baffle is also larger than that for XD-floor, the energy flux density q^{OSP} for XD-shelf is smaller than that for XD-floor at the low upstream densities. As the upstream density, $n_{e,sep}^{OMP}$ increases further, owing to the stronger energy dissipation by neutrals, XD-floor quickly enters detachment, and the corresponding q^{OSP} rapidly decreases, down to the level near the XD-shelf case. As can be seen in figure 11 (b) the rollover of parallel particle flux density occurs at $n_{e,sep}^{OMP} = 0.67\times10^{19}\, m^{-3}$ for XD-floor and $0.94\times10^{19}\, m^{-3}$ for XD-shelf respectively, in spite of the much larger flux expansion of XD-shelf. This clearly shows the strong impact of divertor closure as in the SD cases (Section 3.2). Compared with SD-floor, the density threshold of detachment for XD-floor is even much lower, which indicates that increased divertor closure combined with advanced magnetic configuration, i.e., with larger flux expansion, can further reduce T_e at the target, and hence heat flux density at the divertor target at the same upstream density $n_{e,sep}^{OMP}$, as further discussed in the next section.

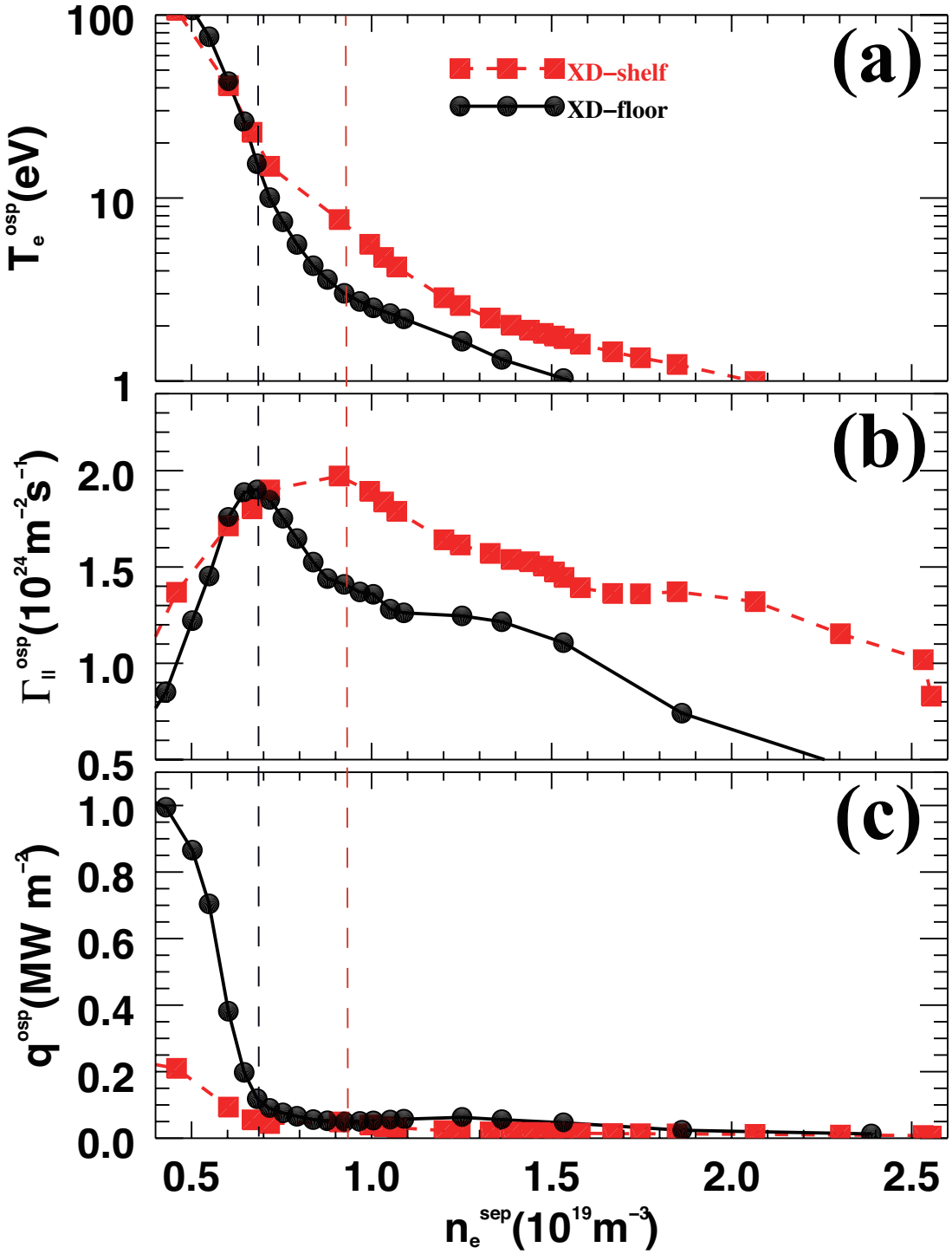

Figure 11. Density scan: (a)T^{osp}, (b)$\Gamma_{||}^{OSP}$, (c) q^{OSP} at the OSP as a function of the upstream density $n_{e,sep}^{OMP}$ for both XD-shelf and XD-floor

3.4. Comparison between SD and XD with different divertor closure

Compared with SD, XD has larger flux expansion, in particular near the divertor target, increasing both the power-dissipating volume in the divertor and the plasma-wetted area on the target surface, thus facilitating divertor detachment [12,27,32]. It is clearly shown in the present calculations that the detachment onset ($0.94\times10^{19}\ m^{-3}$) for XD-

shelf is lower than that ($1.18\times10^{19}\ m^{-3}$) for SD-shelf. Increasing divertor closure reduces the upstream density at the onset of detachment for both SD and XD, with the upstream density at the onset of detachment being lower for XD-floor ($0.67\times10^{19}\ m^{-3}$) than for SD-floor ($0.88\times10^{19}\ m^{-3}$). The densities at the onset of detachment for the XD-floor, SD-floor, XD-shelf and SD-shelf configurations are summarized in Table 1. As can be seen, the modeling shows that coupling of divertor closure and flux expansion in XD-floor enables the divertor plasma to enter detachment at the lowest upstream density among all these different configurations.

Detachment onset	**XD-floor**	**SD-floor**
$n_{e,sep}^{OMP}(10^{19}\ m^{-3})$	0.67	0.88
	XD-shelf	**SD-shelf**
	0.94	1.18

Table 1. Summary of detachment onset for XD-floor, SD-floor, XD-shelf and SD-shelf configurations respectively.

4. Summary

Detailed modeling with SOLPS5.1 in DIII-D has been carried out to assess the synergistic effects of divertor closure and magnetic configuration on divertor detachment, including both open and more closed SD and XD configurations. SOLPS modeling finds that increasing divertor closure with SD reduces the upstream separatrix density at the onset of detachment from $1.18\times10^{19}\ m^{-3}$ for SD-shelf to $0.88\times10^{19}\ m^{-3}$ for SD-floor. Moreover, combing with advanced magnetic configuration further facilitates divertor detachment, with detachment density threshold being reduced down to $0.67\times10^{19}\ m^{-3}$ for the more closed XD-shelf configuration. Modeling also shows that divertor baffling quickly becomes effective at trapping neutrals, hence enhancing power dissipation, as the upstream separatrix increases, despite larger flux expansion associated with XD. These findings indicate that combining divertor closure with advanced magnetic configurations provides a promising means for the design of advanced divertors in the next-step fusion devices.

Acknowledgements

DISCLAIMER: This report was prepared as an account of work sponsored by an agency of the United States Government. Neither the United States Government nor any agency thereof, nor any of their employees, makes any warranty, express or implied, or assumes any legal liability or responsibility for the accuracy, completeness, or usefulness of any information, apparatus, product, or process disclosed, or represents

This work was supported by National Natural Science Foundation of China under Contracts No. 11505234, 11347113, 11575235, 11422546, 11575236, 11675218, 11575244, 11775269; National Magnetic Confinement Fusion Science Program of China under Contracts No. 2015GB101000, 2014GB124006; Scientific Research Grant of Hefei Science Center of Chinese Academy of Sciences under Contract No. 2015SRGHSC008; K.C. Wong Education Foundation; as well as the Thousand Talent Plan of China. This work was also funded by U.S. DOE Contract number DE-FC02-04ER54698. DIII-D data shown in this paper can be obtained in digital format by following the links at https://fusion.gat.com/global/D3D_DMP.

References

[1] Loarte A. 2001 Effects of divertor geometry on tokamak plasmas Plasma Phys. Control. Fusion 43 R183–224

[2] Lipschultz B. et al 2007 Plasma-surface interaction, scrape-off layer and divertor physics: implications for ITER Nucl. Fusion 47 1189-1205

[3] Loarte A. et al 2007 Chapter 4: Power and particle control Nucl. Fusion 47 S203-S263

[4] Stangeby P. C. and Leonard A.W. 2011 Obtaining reactor-relevant divertor conditions in tokamaks Nucl. Fusion 51 063001

[5] Garofalo A. M. et al 2014 Progress in the physics basis of a Fusion Nuclear Science Facility based on the Advanced Tokamak concept Nucl. Fusion 54 073015

[6] Asakura N., et al 2013 A simulation study of large power handling in the divertor for a Demo reactor Nucl. Fusion 53 123013

[7] Guo H. Y. et al 2016 Developing and validating advanced divertor solutions on DIII-D for next-step fusion devices Nucl. Fusion 56 126010

[8] Guo H. Y. et al 2017 Small angle slot divertor concept for long pulse advanced tokamaks Nucl. Fusion 57 044001

[9] Theiler C. et al 2017 Results from recent detachment experiments in alternative divertor configurations on TCV Nucl. Fusion 57 072008

[10] Buttery R. J. and the DIII-D Team 2015 DIII-D research to address key challenges for ITER and fusion energy Nucl. Fusion 55 104017

[11] Kolemen E. et al 2015 Heat flux management via advanced magnetic divertor configurations and divertor detachment J. Nucl. Mater. 463 1186-1190

[12] Covele B. et al 2017 Increased heat dissipation with the X-divertor geometry facilitating detachment onset at lower density in DIII-D Nucl. Fusion 57 086017

[13] Schneider, R., Reiter D., Zehrfeld H. P., Braams B., Baelmans M., Geiger J., Kastelewicz H., Neuhauser J.

and Wunderlich R. 1992 B2-EIRENE simulation of ASDEX and ASDEX-Upgrade scrape-off layer plasmas J. Nucl. Mater. 196–198 810–815

[14] Reiter D. 1992 Progress in two-dimensional plasma edge modelling J. Nucl. Mater. 196–198 80–89

[15] Braams B. J. 1996 Radiative divertor modelling for ITER and TPX Contrib. Plasma Phys. 36 276

[16] Baelmans M., Reiter D. Weynants R. R. 1996 New developments in plasma edge modeling with particular emphasis on drift flows and electric fields Contrib. Plasma Phys. 36 117

[17] Schneider R., Coster D. P., Braams B., Xantopoulos P., Rozhansky V., Voskoboynikov S., Kovaltsova L. and Bürbaumer H. 2000 B2-solsp5.0: SOL transport code with drifts and currents Contrib. Plasma Phys. 40 328-333

[18] Rozhansky V. A., Voskoboynikov S. P., Kaveeva E. G., Coster D. P. and Schneider R. 2001 Simulation of tokamak edge plasma including self-consistent electric fields Nucl. Fusion 41 387

[19] Coster D. P., Bonnin X., Corrigan G., Kirnev G. S., Matthews G., Spence J., Contributors to the EFDA-JET work programme 2005 Benchmarking Tokamak edge modelling codes J. Nucl. Mater. 337–339 366–370

[20] Reiter D., Baelmans M. and Börner P. 2005 The EIRENE and B2-EIRENE codes Fusion Sci. Technol. 47 172-186

[21] Kukushkin A. S., Pacher H. D., Kotov V., Reiter D., Coster D. P. and Pacher G. W. 2005 Effect of neutral transport on ITER divertor performance Nucl. Fusion 45 608–616

[22] Schneider R., Bonnin X., Borrass K., Coster D. P, Kastelewicz H., Reiter D., Rozhansky V. A. and Braams B. J. 2006 Plasma edge physics with B2-Eirene Contrib. Plasma Phys. 46 3–191

[23] Chankin A. V., Coster D. P., Dux R., Fuchs Ch., Haas G., Herrmann A., Horton L. D., Kallenbach A., Kaufmann M., Konz Ch., Lackner K., Maggi C., Müller H. W., Neuhauser J., Pugno R., Reich M., and Schneider W. 2006 SOLPS modelling of ASDEX upgrade H-mode plasma Plasma Phys. Control. Fusion 48 839-868

[24] Kotov V., Reiter D., Pitts R. A., Jachmich S., Huber A., Coster D. P. and JET-EFDA contributors 2008 Numerical modelling of high density JET divertor plasma with the SOLPS4.2 (B2-EIRENE) code Plasma Phys. Control. Fusion 50 105012

[25] Kukushkin A. S., Pacher H. D., Kotov V., Pacher G. W. and Reiter D. 2011 Finalizing the ITER divertor design: The key role of SOLPS modeling Fusion Eng. Des. 86(12) 2865-2873

[26] Canik J. M., Maingi R., Kubota S., Ren Y., Bell R. E., Callen J. D., Guttenfelder W., Kugel H. W., LeBlanc B. P., Osborne T. H. and Soukhanovskii V. A. 2011 Edge transport and turbulence reduction with lithium coated plasma facing components in the National Spherical Torus Experiment Phys. Plasmas 18 056118

[27] Covele B., Valanju P., Kotschenreuther M. and Mahajan S. 2014 An exploration of advanced X-divertor scenarios on ITER Nucl. Fusion 54 072006

[28] Wiesen S., Reiter D., Kotov V., Baelmans M., Dekeyser W., Kukushkin A. S., Lisgo S. W., Pitts R. A., Rozhansky V., Saibene G., Veselova I., Voskoboynikov S. 2015 The new SOLPS-ITER code package J. Nucl. Mater. 463 480-484

[29] Bonnin X., Kukushkin A. S. and Coster D. P. 2009 Code development for ITER edge modelling-SOLPS5.1 J. Nucl. Mater. 390–391 274–277

[30] Garcia-Rosales C., Eckstein W. and Roth J. 1994 Revised formulae for sputtering data J. Nucl. Mater. 218 8-17

[31] Roth J. and Garcia-Rosales C. 1996 Analytic description of the chemical erosion of graphite by hydrogen ions Nucl. Fusion 36 1647–1659

[32] Kotschenreuther M. et al 2013 Magnetic geometry and physics of advanced divertors: the X-divertor and the snowflake Phys. Plasmas 20 102507